EE 256 Final Project Report:
Non-Radiative Mid-Range Wireless Power Transfer

Edwin Ng, Vasu Gupta

June 9, 2014

Abstract

We investigate a scheme for efficient non-radiative mid-range wireless power transfer proposed by Karalis, et al., based on resonant dielectric disks coupled through non-radiative fields near the resonators. We briefly review the efficiency measures for such a power transfer setup, and we present results from a 2D FDFD eigenmode analysis of the coupled disk system. We also show power efficiency calculations from an FDFD analysis of source and load, and investigate the effect of extraneous objects on the system.

1 Introduction

Schemes for wireless power transfer can be loosely classified into three broad categories, based on the length scales involved. Consider the schematic shown in Figure 1 below. The key length scales are the size of the device R_0, the wavelength λ of the electromagnetic waves used, and the separation distance D. In the regime of $D \ll R_0$, we have devices such as transformers; while power transfer is efficient, the large device size is not practical for many purposes. Alternatively, we could also have $D \gg \lambda$ as in directed radiation or lasers; however, these schemes have problems such as radiative loss in the far-field or the need for a clear line of sight. But in the regime where $R_0 < \lambda < D$ (the "mid-range"), a scheme in which the source and load devices can be coupled together selectively and efficiently can be valuable for powering mobile objects, with applications like wireless charging and the operation of robots in factories.
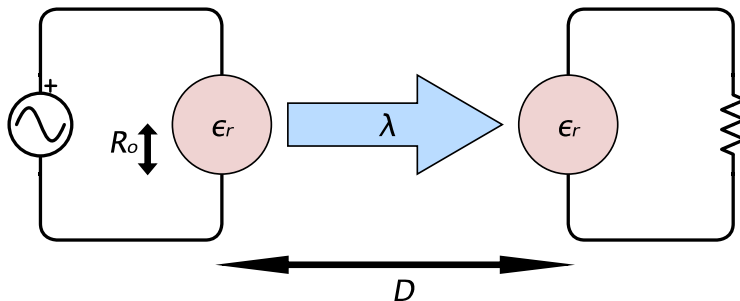

Figure 1: A conceptual schematic showing a general setup for wireless power transfer. The left hand side shows a source driving some device, which then transfers power wirelessly to a corresponding device on the right, connected to a load.

Such a scheme for mid-range power transfer was proposed in 2008 by Karalis, et al. in [1], whose results we explore in this paper. Experimental (and commercial) implementations of these schemes have been realized, such as in [2]; such implementations are also described in detail in [3] and [4].

In Section 2, we briefly review the theory behind achieving selective coupling between two resonant disks and motivate the analysis by presenting measures of transfer efficiency. We present in Section 3 the results of a FDFD-based eigenmode analysis of two dielectric disks as a model system for implementing this scheme. In Section 4, we investigate power flow and transfer efficiency by direct simulation of source and load in the system of coupled disks. We briefly explore the influence of extraneous objects on the system in Section 5, and we conclude by reviewing the efficiencies achieved in this analysis in Section 6.

2 Theory

Fundamentally, in order to model wireless power transfer in a system, we have to solve Maxwell's equations. The requirements for selective, efficient transfer of power, however, suggest that such a scheme can be achieved using the phenomenon of resonance, which we can treat using the approximations provided by coupled mode theory. Suppose that each object m supports a field $\mathbf{E}_m(\mathbf{r})$. Then we can approximate the behavior of the complete system as a time-varying superposition of these individual fields: $\mathbf{E}(t, \mathbf{r}) \approx \sum_m a_m(t) \mathbf{E}_m(\mathbf{r})$. Coupled-mode theory then allows us to approximate the dynamics of this system with the following set of coupled differential equations for the time-varying coefficients $a_m(t)$:

$$\frac{\mathrm{d}a_m(t)}{\mathrm{d}t} = (-\mathrm{i}\omega_m - \Gamma_m)\, a_m(t) + \mathrm{i} \sum_{n \neq m} \kappa_{mn} a_n(t) + F_m(t), \tag{1}$$

where ω_m is the resonant frequency of the isolated object and Γ_m is its intrinsic decay rate to radiation and absorption. The coupling between the objects is modeled by the introduction of the coefficients κ_{mn}, while the term $F_m(t)$ describes the drive imposed on object m. Since the energy density in the system is proportional to $|\mathbf{E}(t, \mathbf{r})|^2$, the energy contained in each object as a function of time evolves as $|a_m(t)|^2$.

Consider now a system of two identical objects, each with a resonance frequency ω and loss rate Γ. Then if we drive object 1 and place a load on object 2 (modeled by a loss rate Γ_{load}), Equation 1 becomes

$$\begin{aligned}
\frac{\mathrm{d}a_1}{\mathrm{d}t} &= (-\mathrm{i}\omega - \Gamma)\, a_1 + \mathrm{i}\kappa a_2 + F e^{-\mathrm{i}\omega_{\text{drive}}t} \\
\frac{\mathrm{d}a_2}{\mathrm{d}t} &= (-\mathrm{i}\omega - \Gamma - \Gamma_{\text{load}})\, a_2 + \mathrm{i}\kappa a_1.
\end{aligned} \tag{2}$$

The energy transfer efficiency η is maximum at $\omega_{\text{drive}} = \omega$, which at steady state is

$$\eta = \frac{\Gamma_{\text{load}} |a_2|^2}{\Gamma |a_1|^2 + (\Gamma_{\text{load}} + \Gamma)|a_2|^2} = \frac{(\Gamma_{\text{load}}/\Gamma)\kappa^2/\Gamma^2}{(1 + \Gamma_{\text{load}}/\Gamma)\kappa^2/\Gamma^2 + (1 + \Gamma_{\text{load}}/\Gamma)^2}. \tag{3}$$

Thus, the loading condition (at resonance) for maximum efficiency is $\Gamma_{\text{load}} = \Gamma\sqrt{1 + \kappa^2/\Gamma^2}$. From this, we can conclude that the optimal efficiency depends only on the ratio κ/Γ.

To determine ω and Γ, we need to find the (complex) eigenfrequency for the isolated disk mode. To determine κ, on the other hand, we make the observation that under $F = 0$ and $\Gamma_{\text{load}} = 0$, Equation 2 admits normal mode solutions at frequencies $\omega \pm \kappa$. This means that we can find κ by finding the eigenfrequencies of the normal modes for the coupled system and computing their frequency splitting.

3 FDFD Eigenmode Analysis of Dielectric Disk System

For our numerical simulations, we consider a system of two dielectric disks as our source and load objects. We implement a 2D TM eigenmode solver in MATLAB, using the FDFD matrix equation

$$-T_{\varepsilon_z}(D_x^b T_{\mu_y}^{-1} D_x^f + D_y^b T_{\mu_x}^{-1} D_y^f)e_z = \omega^2 e_z.$$

We note that the difference matrices D are constructed using SC-PML and so are frequency-dependent. Thus, this is not quite a standard eigenvector problem—we need to provide an initial guess for the frequency.

As a result, the solution process we adopt is the following:

1. Pick an initial guess ω for the frequency, and construct the matrix $A = -T_{\varepsilon_z}(D_x^b T_{\mu_y}^{-1} D_x^f + D_y^b T_{\mu_x}^{-1} D_y^f)$.

2. Compute the eigenvectors of A using MATLAB's `eigs` function for sparse matrices, by supplying it with the initial guess ω^2. This function provides several eigenvectors with eigenvalue close to ω^2.

3. Visually check the output eigenvectors and discard any spurious modes.

We note that the eigenfrequencies found by the eigenmode solver (i.e., the square root of the eigenvalue) are generally complex. The real part corresponds to the resonance frequency ω, while the imaginary part corresponds to the loss rate Γ.
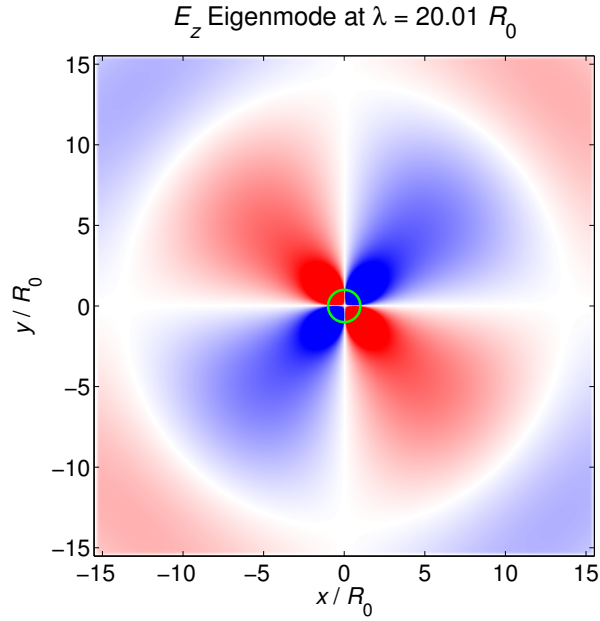
Figure 2: An E_z eigenmode of the isolated disk, with $\lambda \approx 20R_0$. The green circle indicates the location of the dielectric disk. Note that the colorbar is slightly saturated to emphasize the fields outside the disk.

3.1 Eigenmode Calculation of an Isolated Disk

Following [1], we use a relative permittivity of $\varepsilon_r = 147.7\,(1 - \mathrm{i}\,10^{-4})$ for the dielectric disk. For our simulation, we use a grid resolution of 30 pt/R_0, and a PML layer of 15 cells. To compare our results with [1], we look for modes with wavelength $\lambda \approx 20R_0$, providing $\omega = 2\pi c/\lambda$ as our initial guess. The simulation domain (without PML) is $[-0.75\lambda, 0.75\lambda] \times [-0.75\lambda, 0.75\lambda]$.

Figure 2 shows one of the eigenmodes found by our eigenmode solver, corresponding to Fig. 1 in [1]. The eigenfrequency of this mode has real part $\omega = 0.314\,(c/R_0)$ and imaginary part $\Gamma = 0.942 \times 10^{-4}\,(c/R_0)$. The Q-factor of this eigenmode is therefore $Q = \omega/2\Gamma = 1661$, which is in good agreement with the value of 1661 found in Fig. 1 of [1].

3.2 Eigenmode Calculation of a Two Disk System

We next compute eigenmodes of the coupled two disk system, with the same ε_r, guess λ, and simulation domain as above. The disks are oriented along the x axis, with a center-to-center separation D between the disks; we pick $D = 7$ for this section. We use a grid resolution of 15 pt/R_0 and a PML layer of 15 cells.

We identify the normal modes of the system as even and odd superpositions of the isolated disk mode from Figure 2. These modes are plotted in Figure 3. The eigenfrequency for the left normal mode has real part $\omega_1 = 0.3155\,(c/R_0)$ and imaginary part $\Gamma_1 = 0.831 \times 10^{-4}\,(c/R_0)$, while mode on the right has real part $\omega_2 = 0.3159\,(c/R_0)$ and imaginary part $\Gamma_2 = 0.927 \times 10^{-4}\,(c/R_0)$.

The average frequency of these normal modes is therefore $\omega = (\omega_1 + \omega_2)/2 = 0.3157\,(c/R_0)$, while the average loss rate is $\Gamma = (\Gamma_1 + \Gamma_2)/2 = 0.879 \times 10^{-4}\,(c/R_0)$. The frequency splitting can now be found to be $2\kappa = |\omega_1 - \omega_2| = 4.06 \times 10^{-4}\,(c/R_0)$.

We use these averaged quantities to compute the average Q-factor and coupling ratio κ/Γ for $D = 7$. We find $Q = 1796$ and $\kappa/\Gamma = 2.31$, again in good agreement with $Q = 1804$ and $\kappa/\Gamma = 2.3$ found in [1].

3.3 Time Evolution of Normal Modes

Having obtained two normal modes for the coupled disk system, we can also visualize the roles of κ and Γ in energy transfer by looking at the evolution of these normal modes in the time domain. We plot the field

$$\mathbf{E}(t, \mathbf{r}) = e^{\mathrm{i}(\omega_1 + \mathrm{i}\Gamma_1)t}\mathbf{E}_1(\mathbf{r}) + e^{\mathrm{i}(\omega_2 + \mathrm{i}\Gamma_2)t}\mathbf{E}_2(\mathbf{r}),$$

where $\mathbf{E}_1$ and $\mathbf{E}_2$ denotes the electric field of the two modes in Figure 3, respectively.

A movie of $\mathbf{E}$, for the cases of $D = 5R_0$ and $D = 7R_0$, can be accessed at `http://youtu.be/jvZu3ho3XHA`. To remove the fast oscillation at ω, the frames are updated every $2\pi/\omega$. This leaves the beat frequency κ, which we can see is the rate at which the mode moves from one disk to the other and back. Because the system is lossy, the field decays over time at a rate approximately given by Γ.
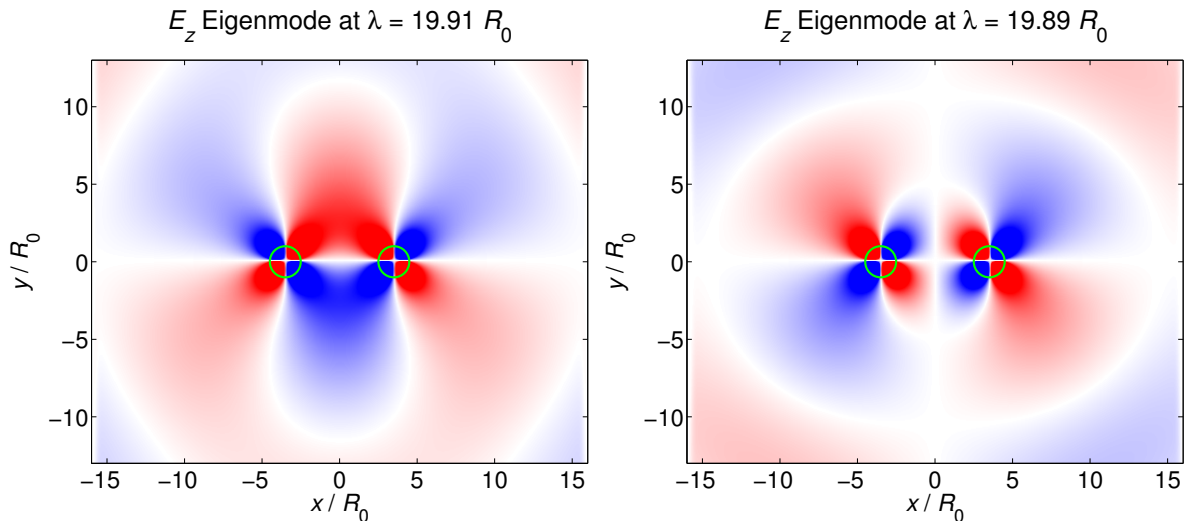
Figure 3: E_z eigenmodes of a coupled two-disk system, with $D = 7R_0$, showing the even (left) and odd (right) normal modes. The green circles indicate the location of the disks, and the color is slightly saturated to emphasize the fields outside the disks. The vertical axis has also been zoomed in to approximately $\pm 0.65\lambda$.

The system $D = 5R_0$ has a coupling ratio $\kappa/\Gamma = 6.5$, while the system $D = 7R_0$ has $\kappa/\Gamma = 2.3$. We see from the movie that this implies the former system can transfer energy between the disks at a faster rate than the latter, confirming that κ/Γ dictates the efficiency of power transfer by prescribing the rate at which energy is moved between the disks, relative to the system losses.

4 FDFD Simulation of System with Source and Load

One way of delivering power from the source to the load is to drive the source with a continuous sinusoidal excitation. We perform an FDFD simulation of the two disk coupled system in order to obtain the power flow in the system under steady state. In this simulation, the drive at the source disk is modeled using a uniform current source density J_z within a circular region of radius $R_0/4$ concentric with the source disk. The load is modeled by increasing the magnitude of the imaginary part of the permittivity of the load disk. In principle, it is possible that such a modification could affect the resonance frequency or the mutual coupling, rather than only introducing Γ_{load}; nevertheless we choose this method for simplicity. Power flow is calculated by computing the power flux using the time-averaged Poynting vector through rectangular regions around the source disk, the load disk, and the periphery (near the PML boundary).

We sweep through a range of drive frequencies ω_{drive} near the (unloaded) resonance frequency ω. At each drive frequency, we compute the power flow through each of the rectangular regions described above, and we plot the results in Figure 4 below, which shows both the case of $D = 7R_0$ and $D = 3R_0$. We can also compute the power transfer efficiency, which we define to be the ratio between the power into the load disk over the power out of the source disk. This is plotted to the right in Figure 4.

We use a resolution of 10 pt/R_0, and a PML layer of 15 cells. The simulation domain is $[-0.5\lambda, 0.5\lambda] \times [-0.5\lambda, 0.5\lambda]$, where again $\lambda = 20R_0$. We use a relative permittivity of $\varepsilon_r = 147.7 \, (1 - \mathrm{i}\, 10^{-4})$ for the source disk (the same as before) but $\varepsilon_r = 147.7 \, (1 - \mathrm{i}\, 10^{-2})$ for the load disk.

5 Influence of Extraneous Objects on Coupled Disk System

Aside from transfer efficiency, a key requirement for efficient power transfer is selectivity—the source and load should not couple strongly to objects other than each other. This is necessary, for example, to prevent leakage of power into other devices, or even to a nearby human user.

To explore the selectivity of the coupled disk system, we look at the eigenmodes of the system when an extraneous object is introduced. We consider a system of three disks, each of radius R_0, with the centers arranged in an equilateral triangle of side length D. We hold the relative permittivity of the two disks on the bottom at $\varepsilon_r = 147.7 \, (1 - \mathrm{i}\, 10^{-4})$. For the top disk, however, we consider two cases: in the first, we set $\varepsilon_r^{\text{obj}} = 49 - 16\mathrm{i}$ (which, according to [1], is a good model for human muscle in the GHz range); in the second, we set $\varepsilon_r^{\text{obj}} = 0.995 \, \varepsilon_r$ (i.e., an object very close to resonance).
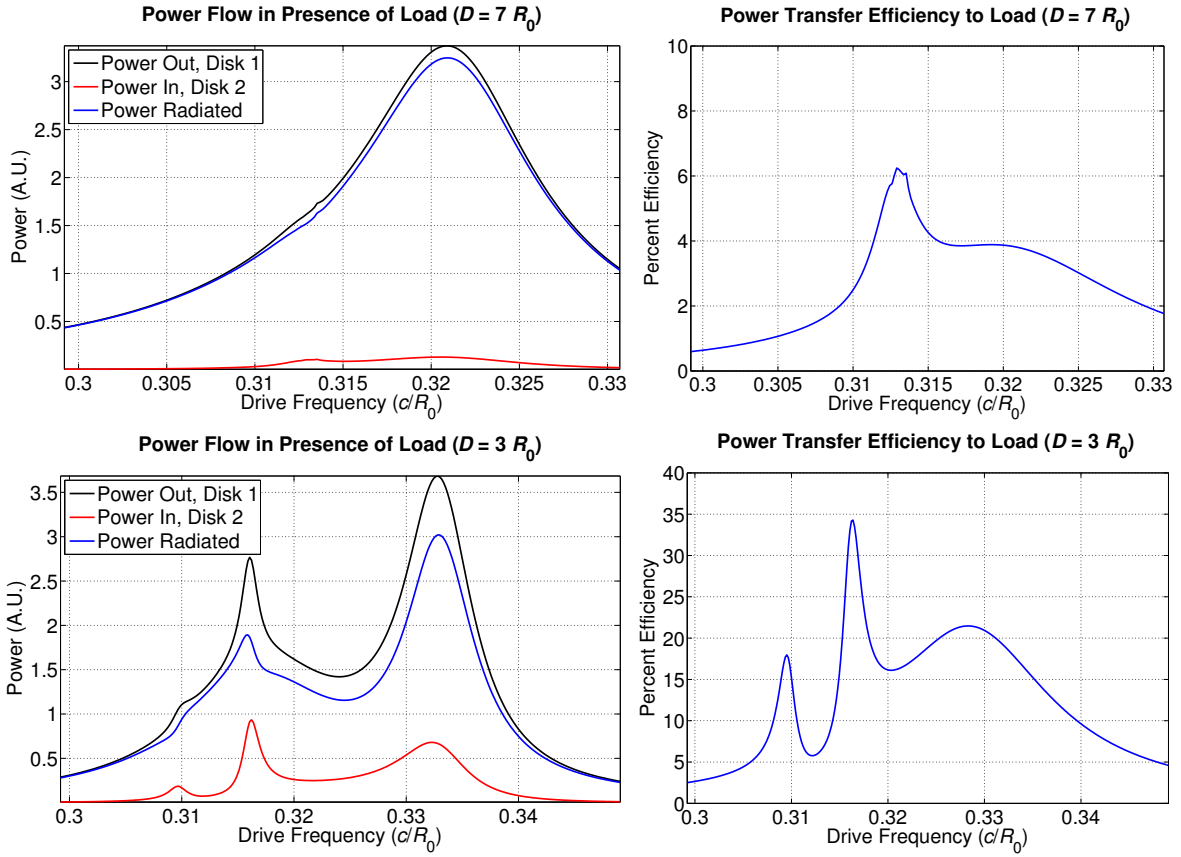
Figure 4: FDFD power flow calculations for the coupled disk system with disk 1 (left disk) as source and disk 2 (right disk) as load, for the cases of $D = 7R_0$ (top) and $D = 3R_0$ (bottom).

We show two eigenmodes, one for each case, in Figure 5 below. We see that in the off-resonance case where $\varepsilon_r^{\mathrm{obj}}$ is far from ε_r, there is minimal field amplitude in the extraneous object. In fact, we can still clearly identify the perturbed normal modes from Figure 3; the coupling ratio is now $\kappa/\Gamma = 2.33$, indicating a minimal effect on the coupling. On the other hand, if $\varepsilon_r^{\mathrm{obj}} \approx \varepsilon_r$, the extraneous object has a very noticeable effect on the eigenmode field pattern, as is evident from Figure 5.
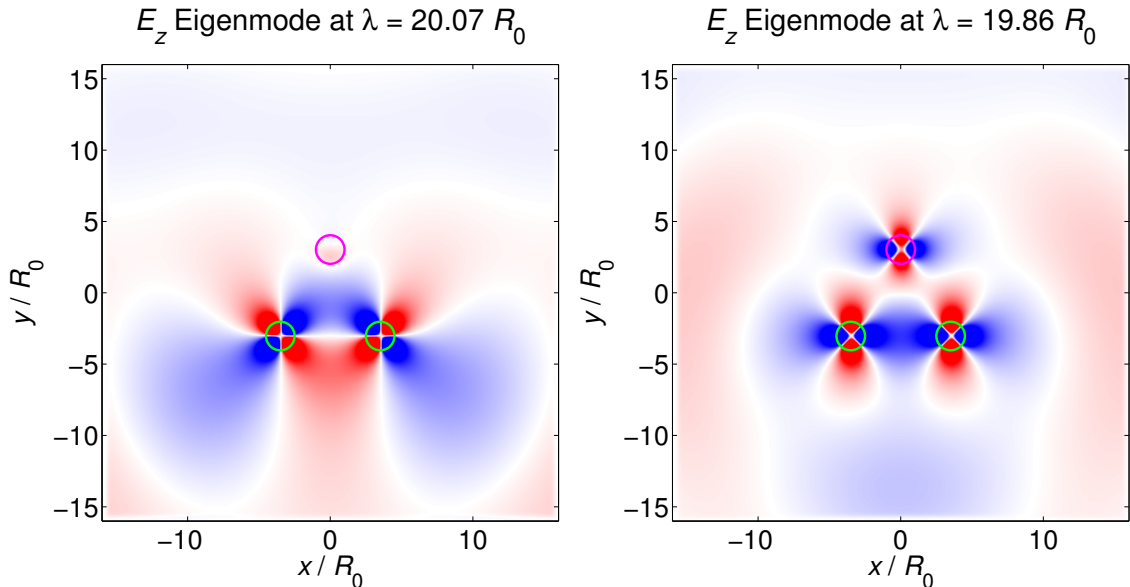

Figure 5: Eigenmodes of the two-disk system in the presence of a perturbing object (a disk of the same size), with mutual separations $D = 7R_0$. On the left, the perturbing disk has $\varepsilon_r^{\mathrm{obj}} = 49 + 16i$, while on the right, the perturbing disk has $\varepsilon_r^{\mathrm{obj}} = 0.995\varepsilon_r$. The green circles indicate the two-disk system, while the magenta circle indicates the perturbing disk. Note that the color is slightly saturated to emphasize the fields outside.

6 Discussion

From the various results above, we can make several conclusions about this proposed scheme for wireless transfer of power in the mid-range. Using the coupling ratios computed from our eigenmode analysis, we can form the plot shown in the left of Figure 6 below. We run the simulation described in Section 3.2 for various values of D, finding that, in the mid-range distances of $D = 3R_0$ up to $D = 12R_0$ (and $\lambda \approx 20R_0$), we have coupling ratios that range from ~ 45 to ~ 0.1. Although this is not quite the regime of $\kappa/\Gamma \gg 1$, it does nevertheless show that wireless transfer of power in the mid-range can be made practical [1].

It is also interesting to see how these coupling ratios correspond to questions about efficiency. The theoretical efficiency curve as a function of κ/Γ (as given by Equation 3) is shown to the right of Figure 6. We also show on this plot the results from our FDFD simulation of source and load, calculated by taking the peak values in the right hand side of Figure 4.
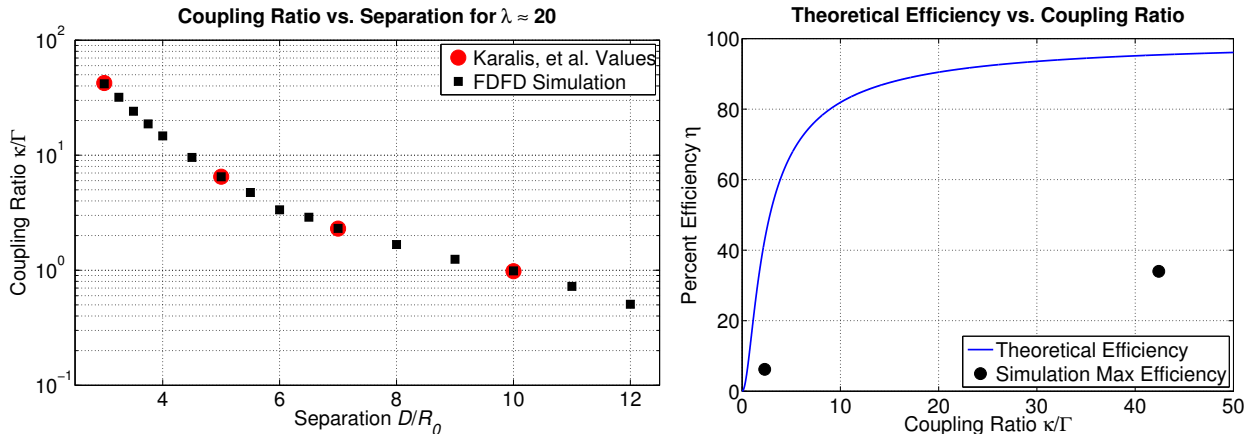

Figure 6: Coupling ratios as a function of separation, and efficiency as a function of coupling ratios. On the left is a plot on a log-scale of the coupling ratios, presented alongside the quoted values from Fig. 2 of [1]. On the right, the theoretical efficiency curve is shown alongside the peak efficiency values from the FDFD simulation of source and load.

The efficiency values obtained from the FDFD simulation are less than the theoretical values, which may be a result of the way we are modeling our load. In our simulations, we could see significant differences in the efficiency if we varied the magnitude of the imaginary part of the load disk's permittivity. This can possibly shift the resonance frequency and the optimal load dissipation rate Γ_{load}, resulting in reduced efficiency. If we use the value for κ/Γ found via eigenmode analysis and assume the theoretical efficiency curve, however, we obtain efficiencies of $\sim 95\%$ (for $D = 3R_0$) to $\sim 45\%$ (for $D = 7R_0$).

The other requirement for efficient (and safe) wireless transfer of power is selectivity in the transfer. In the case of a non-resonant object, we find that the normal modes and the coupling ratios do not vary significantly from the unperturbed values, even when the perturbing object is of the same shape, size, and distance from the coupled resonant system.

7 Conclusions

Following the proposal by Karalis, et al., we investigated an approach to analyze wireless power transfer using FDFD with resonantly coupled dielectric disks. We used an eigenmode analysis to obtain resonant frequencies, losses, and coupling in a system of the coupled disk system, and used these values to evaluate the behavior and performance of the coupled-disk scheme, as well as to verify that the scheme is selective in the transfer. We also performed a basic FDFD simulation of source and load in order to calculate power flow and efficiency in the system, as a complement to the coupled-mode theory approach in Karalis, et al.

The methods used in this report can also be generalized to study wireless power transfer in more general systems, allowing the exploration of varying the material, geometry, etc. of the setup.

In the future, better approaches could be taken to more accurately model the load for our FDFD simulation. Alternative ideas such as FDTD analysis could also be helpful in explicitly simulating power transfer. In this latter scheme, it may also be interesting to study the effect of different schemes for excitation (such as pulsing rather than sinusoidal drive), as well as perhaps time dependent material properties or geometry (as in moving targets, etc.).

References

[1] A. Karalis, J.D. Joannopoulos, and M. Soljačić. "Efficient Wireless Non-radiative Mid-range Energy Transfer". *Annals of Physics*, **323** 34–48 (2008).

[2] A. Kurs, A. Karalis, R. Moffatt, J.D. Joannopoulos, P. Fisher, and M. Soljačić. "Wireless Power Transfer via Strongly Coupled Magnetic Resonances". *Science*, **317** 5834 (2007).

[3] R. Moffatt. *Wireless Transfer of Electric Power*. S.B. thesis, Massachusetts Institute of Technology, 2009.

[4] A. Kurs. *Power Transfer Through Strongly Coupled Resonances*. S.B. thesis, Massachusetts Institute of Technology, 2007.